

Anisotropic Intermolecular Interactions and Through-Space/Through-Bond Intramolecular Interactions Observed by Collision-Energy-Resolved Penning Ionization Electron Spectroscopy

Naoki Kishimoto, Hideyuki Ogasawara, and Koichi Ohno*

Department of Chemistry, Graduate School of Science, Tohoku University, Aoba-ku, Sendai, 980-8578

(Received February 14, 2002)

Ionization of 1,4-diazabicyclo[2.2.2]octane (DABCO), 1,4-cyclohexadiene (CHD), and 2,5-norbornadiene (NBD) with $He^*(2^3S)$ metastable atoms was studied by (collision-energy/electron-energy-resolved) two-dimensional Penning ionization electron spectroscopy. Anisotropic interaction around the molecule was investigated by determining collision energy dependence of partial ionization cross sections (CEDPICS) and spatially anisotropic distribution of ionized molecular orbitals (MOs). The negative slope of CEDPICS for HOMO was smaller than that for the next HOMO of DABCO and CHD; this was due to the repulsive interaction around the $\sigma_{CC,CH}$ bond region, which is related to the through-bond interaction via the electron distribution. The trend of CEDPICS for DABCO was confirmed by classical trajectory calculations. For NBD, the negative CEDPICS for the next HOMO was larger than that for HOMO; this was due to the attractive endo region for the in-phase next HOMO with the through-space interaction.

Since the reactivity and chemical behavior of a molecule have strong relation to the electron density distribution of specific molecular orbitals (MOs) as known in Fukui's frontier orbital theory,[1] the orbital reactivity of the molecule plays an important role in intermolecular processes including chemical reactions. In the frontier orbital theory, the energy of MOs is also an important factor in interorbital interactions. Regarding the orbital energy levels, the energetic relationship between plural π or nonbonding orbitals has been studied with the help of a concept of through-bond/through-space intramolecular interactions.[2] To examine the interactions between two π or nonbonding orbitals in a molecule, photoelectron spectroscopy[3,4] as well as theoretical calcuations[5] were applied for determination of the highest occupied MO (HOMO) and the next HOMO (NHOMO) of 1,4-diazabicyclo[2.2.2]octane (DABCO), 2,5-norbornadiene (NBD), and 1,4-cyclohexadiene (CHD).

In Penning ionization ($M + He^*(2^3S) \rightarrow M^+ + He + e^-$) process, an electron in a molecular orbital of M is transferred to the lowest vacant orbital of He^*, and the excited electron from He^* is ejected.[6] The probability of the electron transfer, therefore, mainly depends on the spatial overlap between the orbitals of M and He^*. Penning ionization electron spectroscopy[7–9] provides us information on the spatial electron distribution of individual molecular orbitals in the frontier region outside the molecular surface (boundary surface of collision between a molecule M and $He^*(2^3S)$).[10] In order to estimate the orbital reactivity, an exterior electron density (EED) model[10] was proposed. In the EED model, orbital reactivity was simply governed by the electron density extending outside the molecular surface, assuming head-on collisions with the hard sphere. This model was successfully applied to estimation of the orbital reactivity of hydrocarbon molecules,[11–13] ethly chloride,[11] $(CH_3)_4M$ (M = C, Si, Ge, Sn, Pb),[14] DABCO,[11,15] CHD,[15] and NBD.[11,15] For DABCO and NBD, the symmetric or anti-symmetric combination of MOs by the through-bond/through-space interaction was determined from the difference in band intensity for HOMO and NHOMO.[11,15]

On the other hand, collision-energy/electron-energy-resolved (two-dimensional) measurements[16] of Penning ionization enabled us to measure collision energy dependence of the partial ionization cross sections (CEDPICS). The different trends of CEDPICS indicate the anisotropic interactions around the molecule with $He^*(2^3S)$ atoms. Recently, we have studied anisotropic interaction between $He^*(2^3S)$ atoms and orbital reactivity of halogen atoms for halogeno ethylenes and halogeno benzenes.[17] In the case of molecules having relation with the through-bond/through-space interaction, different trends of CEDPICS for HOMO and NHOMO indicate not only symmetry of orbitals but also a slight difference in spatial electron distribution of the two MOs around the bond or spatial region which is connected to the through-bond/through-space interaction. In this study, we investigated two-dimensional Penning ionization electron spectra (2D-PIES) of DABCO, CHD, and NBD.

Experimental

The experimental apparatus for $He^*(2^3S)$ Penning ionization electron spectra (PIES) and He I ultraviolet photoelectron spectra (UPS) was reported previously.[18–20] Metastable atoms of $He^*(2^1S, 2^3S)$ were produced by a discharge nozzle source with a hollow tantalum cathode. The $He^*(2^1S)$ component was quenched by a water-cooled helium discharge lamp. The background pressure in a reaction chamber was on the order of 10^{-7} Torr. Sample molecules were admitted by a variable leak valve into a reaction chamber. He I UPS of these samples were measured by using the He I

resonance photons (584 Å, 21.22 eV) produced by a discharge in pure helium gas. The kinetic energy of ejected electrons was measured by a hemispherical electrostatic deflection type analyzer using an electron collection angle 90° to the incident $He^*(2^3S)$ or photon beam. The energy resolution of the electron energy analyzer was estimated to be 60 meV from the full width at half-maximum (fwhm) of the $Ar^+(^2P_{3/2})$ peak in the He I UPS. The transmission efficiency curve of the electron energy analyzer was determined by comparing our UPS data for some molecules with those by Gardner and Samson[21] and Kimura et al.[22] Calibration of electron energy scale was made by reference to the lowest ionic state of N_2 mixed with the sample molecule in He I UPS (E_e = 5.639 eV)[23] and $He^*(2^3S)$ PIES (E_e = 4.292 eV)[24,25] including a peak energy shift of 50 meV and the difference between the metastable excitation energy and the lowest ionization potential (IP).

For collision-energy-resolved measurements of Penning ionization, the metastable $He^*(2^3S)$ beam was modulated by a pseudo-random chopper[26] rotating at 400 Hz, and then introduced into a reaction cell located 504 mm downstream from the chopper disk. Kinetic energies and time-dependent counts of emitted electrons from sample molecules were stored in a memory. The resolution of the analyzer was lowered to 250 meV in order to obtain higher counting rates of Penning electrons. Two-dimensional spectra $I_e(E_e, t)$ as functions of electron kinetic energy (E_e) and time (t) can lead to the two-dimensional Penning ionization cross section $\sigma(E_e, E_c)$ as functions of E_e and E_c (collision energy) normalized by the velocity distribution of the He^* beam. The velocity distribution of He^* beam was determined by monitoring secondary electrons emitted from a stainless plate inserted in the reaction cell.

Calculations

We performed ab initio self-consistent field (SCF) calculations in order to obtain electron density maps. The geometries of neutral target molecules were selected from previous studies for DABCO,[27] CHD,[28] and NBD.[29] In electron density contour maps, thick solid curves indicate the repulsive molecular surface approximated by atomic spheres of van der Waals radii.[30] In schematic diagrams of molecular orbitals, circles and ellipses were used. Solid circles indicate valence s orbitals, where couples of ellipses and dashed circles showed in-plane and out-of-plane components of p orbitals, respectively. Ionization potentials (IP) were calculated by the outer valence Green's function (OVGF)[31] method in GAUSSIAN 94 program.[32] The SCF and OVGF calculations were performed with 6-311++G** and 6-311G** basis functions, respectively.

Interaction potential energies between $He^*(2^3S)$ and the targets for various directions were also calculated on the basis of the well-known resemblance[33] between $He^*(2^3S)$ and $Li(2^2S)$; the shape of the velocity dependence of the total scattering cross section of $He^*(2^3S)$ by He, Ar, and Kr is very similar to that of Li, and the location of the interaction potential well and its depth are very similar for $He^*(2^3S)$ and $Li(2^2S)$ with various targets.[7,34–37] For atomic targets (H, Li, Na, K, and Hg), quantitative estimation of the well depth was summarized to be in good agreement with the ratio of 1.1 to 1.2 by Li model potential with respect to $He^*(2^3S)$ in a recent study.[38] Due to these findings and difficulties associated with calculations for excited states, the Li atom was used in place of $He^*(2^3S)$ atom. We performed interaction potential energy calculations for access of Li atom to the molecule from various directions using a second-order Møller–Plesset perturbation theory (MP2). For discussing peak energy shift and bandwidth broadening of first ionic state (X state) in PIES of DABCO, potential energy curves of the ionized DABCO with a He atom were calculated by the Hartree–Fock method. The interaction potential calculations were carried out with 6-31+G* basis functions.

Trajectory calculations for ionization of DABCO were performed on a three-dimensional potential energy surface obtained by the MP2 method. The cubic spline interpolation calculations were utilized for more than 300 points with D_{3h} symmetry of the molecule. Ionization width was calculated on the following simplification:[39] since the positional dependence of the ionization width Γ is mainly governed by the helium 1s and ionized orbitals, the ionization widths for each ionic state $\Gamma^{(i)}$, therefore, are represented by

$$\Gamma^{(i)} = K\,|<\Phi_i|\Psi_{1s}>|^2 \tag{1}$$

where K is a constant, and Φ_i and Ψ_{1s} are the ionized MO and helium 1s orbital, respectively. The molecule is treated as a rigid rotator. The orientation of DABCO was randomly generated, and the initial rotational energy of the molecule was determined with a Boltzmann distribution at 300 K. The impact parameter b was set randomly from 0 to 8 Å for 10000 trajectories at each collision energy (70, 100, 150, 200, 250, and 280 meV). The partial ionization cross section $\sigma^{(i)}$ was obtained from ionization probability $P^{(i)}$ with a weight of $2\pi bdb$.

$$\sigma^{(i)} = 2\pi\int bP^{(i)}db \tag{2}$$

Details of the trajectory calculations were reported in previous papers.[39] Several K values were attempted for better agreement of the slope of CEDPICS, because the determination of the unknown K value requires an experimental value of ionization cross section.

Results

Figures 1–3 show the He I UPS and $He^*(2^3S)$ PIES of DABCO, CHD, and NBD, respectively. The electron energy scales for PIES are shifted relative to those for the UPS by the difference in the excitation energies, 21.22 − 19.82 = 1.40 eV. In Fig. 1, the EED spectrum of band 1 is shown in the inset, and details for the synthesis of the band shape are written in the Discussion Section.

Figures 4–6 show CERPIES of DABCO, CHD, and NBD, respectively. In each figure, the low collision energy (average ca. 100 meV) spectra are shown by solid curves, and the high collision energy (average ca. 250 meV) spectra are shown by dashed curves. In Fig. 4, band 1 and band 2 are shown in an inset as a function of peak energy shift in PIES measured with respect to the "nominal" energy E_0 (= the difference between the metastable excitation energy and the target IP).

Figures 7–9 show the log σ vs log E_c plots of CEDPICS for DABCO, CHD, and NBD, respectively. The CEDPICS were obtained from the 2D-PIES within an appropriate range of E_e (typically the fwhm of the respective band) to avoid the effect of neighboring bands. Solid lines in Fig. 7 showed the calculated CEDPICS for DABCO. The calculated electron density

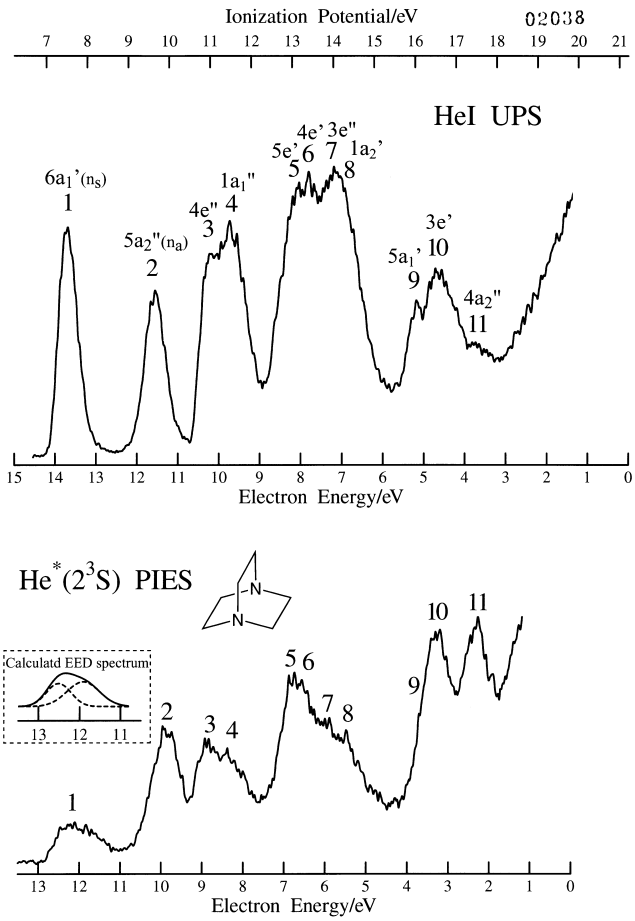

Fig. 1. He I ultraviolet photoelectron spectrum and $He^*(2^3S)$ Penning ionization electron spectrum of DABCO. The calculated EED spectrum was also shown in the inset (see text).

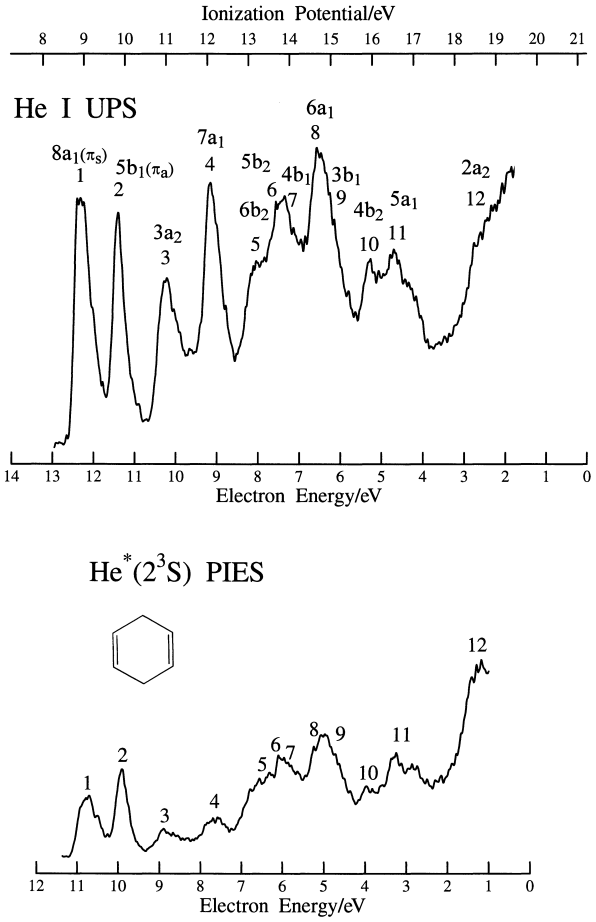

Fig. 2. He I ultraviolet photoelectron spectrum and $He^*(2^3S)$ Penning ionization electron spectrum of 1,4-cyclohexadiene.

maps of the MOs are also shown in the figures with the simplified diagrams indicating component atomic orbitals.

Tables 1 and 2 list the vertical ionization potentials (IP determined from the He I UPS) and assignment of the observed bands based on the OVGF calculations. The peak energy shifts (ΔE) in PIES with respect to E_0 are also shown. The values of peak energy shift of some diffuse bands or shoulders are shown in parentheses. Values of the slope parameter m for the $\log\sigma$ vs $\log E_c$ plots were estimated in the collision energy range 100–240 meV by a least-squares method.

Figures 10–12 show model potential energy curves $V(R)$ determined by MP2 method for M(DABCO)-Li, M(CHD)-Li, and M(NBD)-Li, respectively. The curves were obtained by a spline interpolation method. The distance R between the target molecule and Li is measured from the center-of-mass for DABCO and CHD except for the access of Li to the C atom of the CH_2 group for DABCO and to the middle point of C=C group of CHD. For NBD, R is measured from the C atom of methylene bridge or the middle point of the C=C bond. In Fig. 12(b), the interaction potential energy curve $V(\theta)$ as a function of angle θ between Li-X (X is the middle point of C=C) and the H–C=C–H plane is also shown. A hump in the curve around 0 degrees is due to repulsive interaction around H atoms. In Fig. 10(b), the interaction potential energy curves of the first ionized state of M^+(DABCO)–He are also shown. In Fig. 10(c), the contour map of interaction potential energy calculations for M(DABCO)-Li is shown.

Discussion

A. 1,4-Diazabicyclo[2.2.2]octane. By an SCF MO calculation and use of an OVGF method, band 1 and band 2 were assigned to ionization from $6a_1'$ (symmetric nonbonding MO, n_s) and $5a_2''$ MO (asymmetric nonbonding MO, n_a), respectively. If the direct through-space interaction between nonbonding orbitals on two nitrogen atoms dominates the orbital energy (ε) order, the symmetric n_s MO is more stable than the asymmetric n_a MO ($\varepsilon(n_a) > \varepsilon(n_s)$). In the case of DABCO, however, the through-bond interaction between nonbonding orbitals on two distant nitrogen atoms dominates[3b] the orbital energy order for HOMO and NHOMO, $\varepsilon(n_s) > \varepsilon(n_a)$. In addition, for the n_s orbital, some anti-bonding mixing of σ_{CC} components with n_s orbital was seen in $6a_1'$ as shown in the electron density map in Fig. 7, which results in the band intensity of band 1 in PIES being relatively smaller than that of band 2, as calculated by the EED model.[11,15] The EED values for n_s and n_a orbitals outside the molecular surface approximated by the van der Waals surface were calculated with the 6-311++G** basis set to be

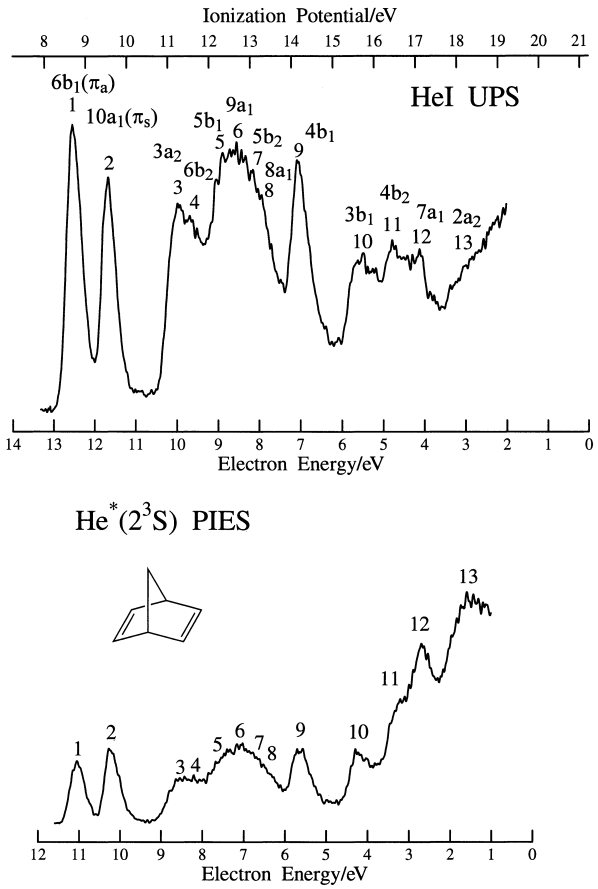

Fig. 3. He I ultraviolet photoelectron spectrum and He*(2^3S) Penning ionization electron spectrum of 2,5-norbornadiene.

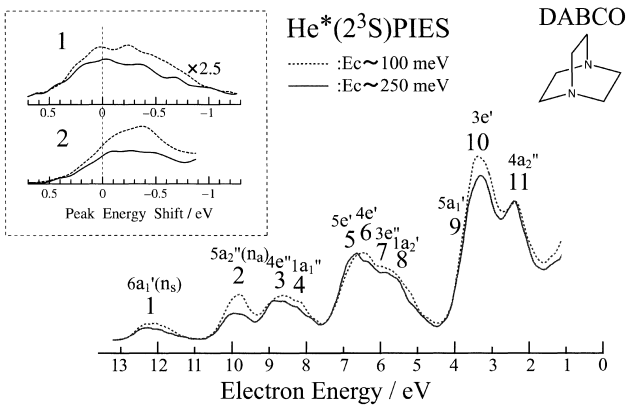

Fig. 4. Collision-energy-resolved Penning ionization electron spectrum for DABCO with He*(2^3S): dotted line at average energy of 100 meV and solid line at average energy of 250 meV. Band 1 and band 2 are also shown as a function of peak energy shift with respect to "nominal" energy determined by ionization potentials in an inset. The intensity of band 1 is shown 2.5 times as large as the case of band 2.

3.36 and 4.01, respectively. For a good agreement of EED ratios with the PIES result, diffuse functions in basis set at SCF molecular orbital calculations were found to be important.[12,40]

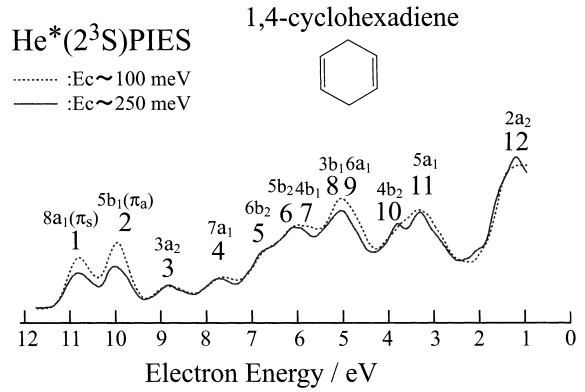

Fig. 5. Collision-energy-resolved Penning ionization electron spectrum for 1,4-cyclohexiadiene with He*(2^3S): dotted line at average energy of 100 meV and solid line at average energy of 250 meV.

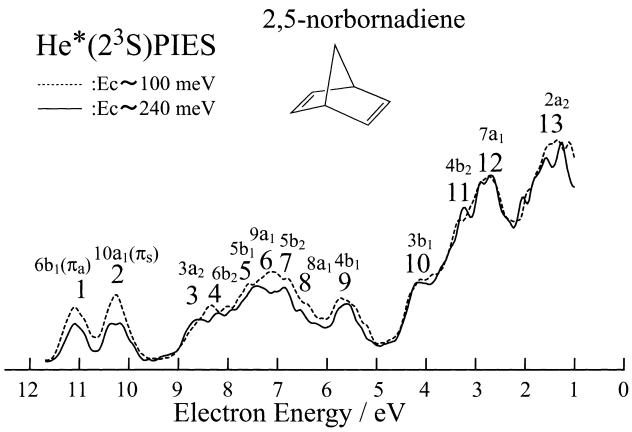

Fig. 6. Collision-energy-resolved Penning ionization electron spectrum for 2,5-norbornadiene with He*(2^3S): dotted line at average energy of 100 meV and solid line at average energy of 240 meV.

It should be noted that the outermost two symmetric or antisymmetric orbitals of DABCO, NBD, and CHD were observed[41] with (e, 2e) electron momentum spectroscopy[42] and these results confirmed the importance of diffuse functions in basis sets.

A negative slope of CEDPICS was observed for band 1 ($m = -0.40 \pm 0.04$) and band 2 ($m = -0.51 \pm 0.07$). For an attractive interaction between the molecule and a He* atom, a slower atom can reach to reactive region around the molecule more effectively than faster He* atoms, which results in a large ionization cross section for small collision energy and negative slope of CEDPICS. Opposite to the attractive interaction, a repulsive interaction results in a positive slope of CEDPICS because reaching the inner reactive region of the molecule is more possible for faster He* atoms than for slower He* atoms.[18] The negative slope of CEDPICS for band 1 and band 2 indicates an attractive interaction around the nitrogen lone pair orbital region. Indeed, as shown in Fig. 10, the calculated interaction potential curve for the access along the symmetry axis shows an attractive interaction with the well depth of 600 meV.

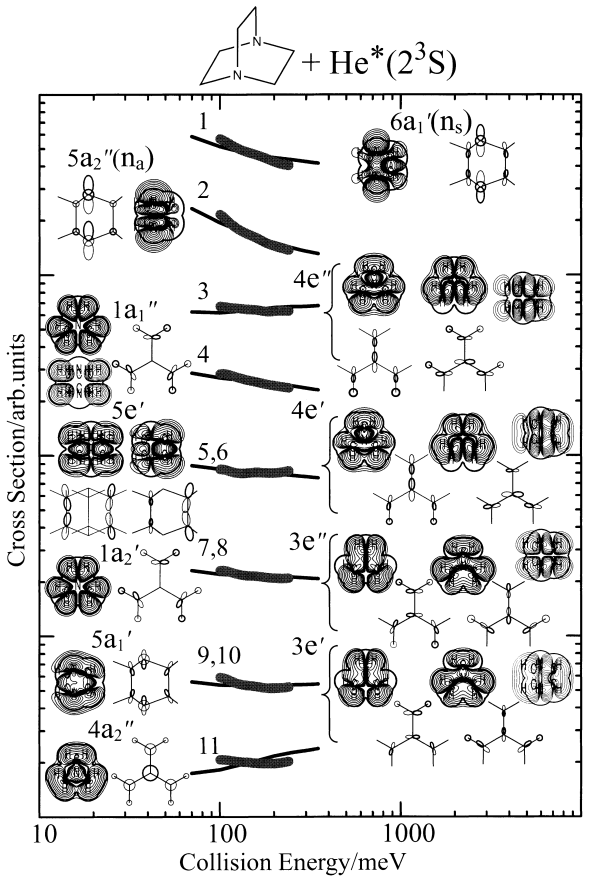

Fig. 7. Collision energy dependence of partial ionization cross sections for DABCO with $He^*(2^3S)$. Electron density maps for respective MOs are also shown on a plane including an NCCN bond for $6a_1'$, $5a_2''$, $5e'$, $4e''$, $4e'$, $3e''$, $3e'$, and $5a_1'$ MOs, on a plane including four C atoms for $1a_1''$ and $5e'$ MOs, and on a plane including three C atoms for $1a_1''$, $4e''$, $4e'$, $3e''$, $3e'$, $1a_2'$, and $4a_2''$ MOs. Thick solid curves in the maps indicate the simple estimation of the repulsive surface from spheres of van der Waals radii.

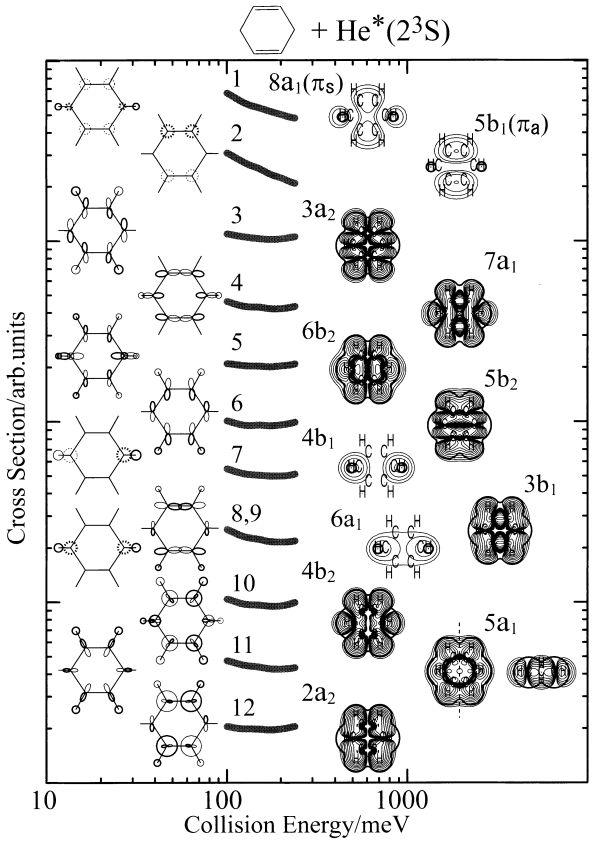

Fig. 8. Collision energy dependence of partial ionization cross sections for 1,4-cyclohexiadiene with $He^*(2^3S)$. Electron density maps for respective MOs are also shown on a plane at 2 Å from the molecular plane for $8a_1$, $5b_1$, $4b_1$, and $6a_1$ MOs and on the molecular plane for other MOs. Thick solid curves in the maps indicate the simple estimation of the repulsive surface from spheres of van der Waals radii.

By the trajectory calculation on the interaction potential energy surface (Figs. 10(a) and (c)), a steeper slope of CEDPICS for the n_a orbital (band 2) rather than for the n_s orbital (band 1) was calculated, which agrees better with the observed slope of CEDPICS. Since the positive or negative trend of CEDPICS reflects the deflection of He^* by repulsive or attractive interactions, the slope value of CEDPICS shows the extent of influence on trajectories of He^* atoms by interactions if the corresponding MO extends in both repulsive and attractive interaction regions. Therefore, the difference between the negative slope of CEDPICS for band 1 ($m = -0.40 \pm 0.04$) and that of band 2 ($m = -0.51 \pm 0.07$) can be ascribed to the repulsive interaction around the σ_{CH} bonds for ionization from the $6a_1'$ orbital (band 1) calculated for the straight access to the H atom (Fig. 10). In this study, from the points of the anisotropic electron density distribution of MOs and the anisotropic interactions around the molecule, we have confirmed that the X and A ionic states are due to ionization from n_s and n_a MOs, respectively. By the (e, 2e) electron momentum spectroscopy, different momentum profiles reflecting the different symmetry of HOMO ($6a_1'$) and NHOMO ($5a_2''$) were observed.[41b] On the other hand, in the case of collision-energy-resolved Penning ionization electron spectroscopy, the electron distribution of HOMO in the position space results in different CEDPICS from that of NHOMO due to the electron distribution around the σ_{CH} bonds. It should be noted that the extension of wave functions can be sensitively observed by (e, 2e) electron momentum spectroscopy, while CEDPICS is mainly affected by the anisotropic distribution of MOs in the position space and by the interaction potential around the molecule. The quantitative agreement between observed and calculated CEDPICS can be achieved by trajectory calculations on the interaction potential energy surface, in which the effects of electron correlations and electron transfer from He^*(Li) to unoccupied MOs are taken into consideration.[39]

The electron energy in PIES shows some interaction energy difference in entrance channel and exit channel at reaction points.[7,8] With the help of the calculated well depth (ca. 600 meV at $R = 3.5$ Å) of the entrance channel and the height of the wall (ca. 200 meV at $R = 3.5$ Å) for the first ionic state (exit channel) as shown in Fig. 10, a peak energy shift for ionization around N atoms can be estimated as ca. −400 meV. In ad-

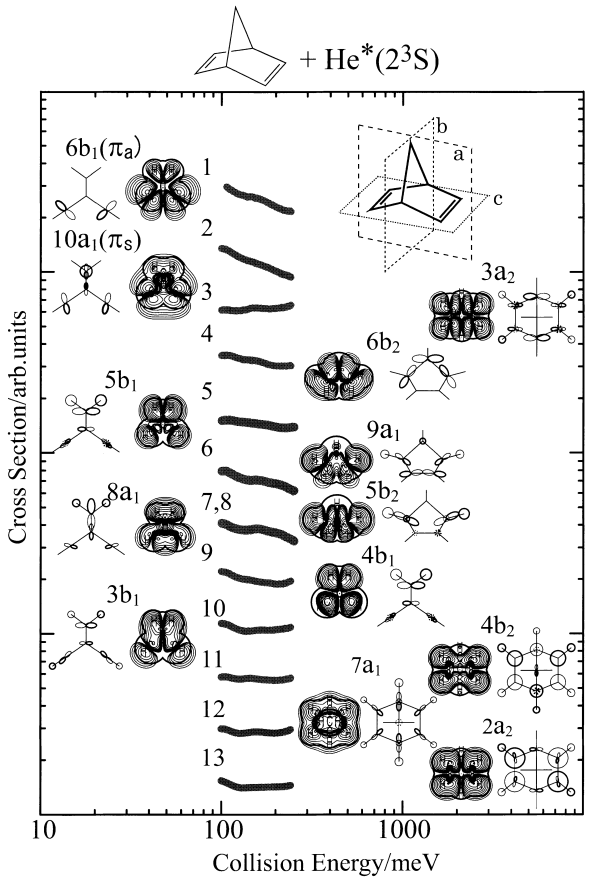

Fig. 9. Collision energy dependence of partial ionization cross sections for 2,5-norbornadiene with $He^*(2^3S)$. Electron density maps for respective MOs are also shown: on a plane (a) including CH_2 group for $6b_1$, $10a_1$, $5b_1$, $8a_1$, $4b_1$, and $3b_1$ orbitals; on a plane (b) including H–C–C–C–H atoms for $6b_2$, $9a_1$, and $5b_2$ orbitals; on a plane (c) including four C atoms for $3a_2$, $4b_2$, $7a_1$, and $2a_2$ orbitals. Thick solid curves in the maps indicate the simple estimation of the repulsive surface from spheres of van der Waals radii.

dition, a positive peak energy shift can be expected for ionization around σ_{CH} bonds from the soft repulsive interaction for the entrance channel and steep repulsive interaction for the exit channel, as shown in Fig. 10. Band 1 in PIES (Fig. 1) shows a broadened bandwidth compared with that of band 2. The EED spectrum of band 1 in the inset to Fig. 1 was synthesized by utilizing the estimated peak energy shifts for ionization at N atoms (−400 meV) and H atoms (+200 meV) and the EED values of $6a_1'$ MO at N atoms (1.78) and H atoms (1.24) with assuming a Gaussian function. For larger electron energy component, we adopted the value of 600 meV for band width (fwhm), which is larger than that of band 1 (ca. 500 meV) in He I UPS because of the collisional ionization process on the anisotropic interaction potential with transition probability extending around the molecule. Since transition processes around an attractive interaction potential well around N atoms can result in a larger band width than that for repulsive interactions, the value of 800 meV was adopted for band width of a smaller electron energy component. The synthesized band shows a good agreement with the observed band shape. In addition, different collision energy dependences in higher electron energy region ($m = -0.35 \pm 0.02$) and in lower electron energy region ($m = -0.43 \pm 0.05$) were observed for band 1 of CERPIES (Fig. 4). If one takes the shapes of entrance and exit potential energy curves into consideration, the different tendencies of CEDPICS and CERPIES in higher and lower electron energy regions correspond to ionization in the repulsive region around the σ_{CH} bonds and in the attractive region around the N atoms, respectively.

For band 2, the shape of CERPIES at $E_c \sim 100$ meV shows large intensity in lower electron energy region with a negative peak shift of ca. −400 meV. This shift value is consistent with deep potential wells for the n_N orbital region. That the negative peak energy shift for band 2 is larger than that for band 1 observed in CERPIES (as inserted in Fig. 4), therefore, indicates that ionization from n_a orbital mainly occurs in the attractive region around N atoms. On the other hand, the bent figure of observed and calculated CEDPICS for band 1 and band 2 due to the increase of ionization cross sections in larger collision energy regions may be due to trajectories of He^* ionized against the repulsive interaction around methylene groups where corresponding MOs extend.

An attractive interaction around N atoms affects the negative slope of band 5,6 ($5e'$ and $4e'$ MOs, $m = -0.03 \pm 0.05$) and band 9,10 ($5a_1'$ and $3e'$ MOs, $m = -0.16 \pm 0.08$) because

Table 1. Band Assignments, Ionization Potential (IP/eV), Peak Energy Shift (ΔE/meV), and Slope Parameter (m, See Text) for 1,4-Diazabicyclo[2.2.2]octane (DABCO)

Band	IP/eV Obsd	IP/eV Calcd	Orbital	ΔE/meV	m Obsd	m Calcd
1	7.51	7.34	$6a_1'$ (n_s)	−200 ± 100	−0.40 ± 0.04	−0.18
2	9.67	9.63	$5a_2''$ (n_a)	−260 ± 50	−0.51 ± 0.07	−0.35
3	11.01	11.36	$4e''$ (σ_{CH}, σ_{CN})	50 ± 80	−0.08 ± 0.02	0.09
4	11.47	11.69	$1a_1''$ (σ_{CH})	30 ± 80	−0.23 ± 0.02	−0.11
5	13.01	12.98	$5e'$ (σ_{CC})	−60 ± 80	−0.03 ± 0.05	−0.10
6	13.41	13.47	$4e'$ (σ_{CN})	−70 ± 80		−0.03
7	14.02	14.15	$3e''$ (σ_{CH}, σ_{CN})	50 ± 100	−0.13 ± 0.05	−0.10
8	14.28	14.15	$1a_2'$ (σ_{CH})	−60 ± 100		0.06
9	16.04	16.11	$5a_1'$ (π_{CN})	−100 ± 200	−0.16 ± 0.08	−0.10
10	16.54	16.63	$3e'$ (σ_{CH}, σ_{CC})	−70 ± 100		0.12
11	17.49	17.43	$4a_2''$ (C_{2s}, N_{2s})	−60 ± 100	(0.0)	0.24

Table 2. Band Assignments, Ionization Potential (IP/eV), Peak Energy Shift (ΔE/meV), and Slope Parameter (m, See Text) for 1,4-Cyclohexadiene (CHD) and 2,5-Norbornadiene (NBD)

Band	IP_{obsd}/eV	IP_{calcd}/eV	Orbital	ΔE/meV	m
1,4-Cyclohexadiene					
1	8.92	8.79	$8a_1(\pi_s)$	-160 ± 50	-0.35 ± 0.04
2	9.83	9.60	$5b_1(\pi_a)$	-80 ± 50	-0.44 ± 0.03
3	11.01	11.02	$3a_2(\sigma_{CH}, \sigma_{CC})$	70 ± 80	-0.06 ± 0.05
4	12.07	12.05	$7a_1(\sigma_{CC})$	-150 ± 100	-0.08 ± 0.06
5	13.18	13.20	$6b_2(\sigma_{CH}, \sigma_{CC})$	-20 ± 100	-0.01 ± 0.04
6	13.67	13.70	$5b_2(\pi_{CH_2})$	-10 ± 100	-0.02 ± 0.05
7	13.97	14.14	$4b_1(\pi_{CC})$	(0 ± 100)	-0.09 ± 0.05
8	14.66	14.58	$6a_1(\pi_{CH_2})$	-100 ± 150	-0.18 ± 0.07
9	15.08	14.97	$3b_1(\sigma_{CH}, \sigma_{CC})$	(0 ± 100)	
10	15.96	16.12	$4b_2(C_{2s})$	90 ± 80	-0.07 ± 0.05
11	16.53	16.68	$5a_1(\sigma_{CH})$	-40 ± 50	-0.09 ± 0.04
12	18.6	18.91	$2a_2(C_{2s})$	—	(0.0)
2,5-Norbornadine					
1	8.68	8.28	$6b_1(\pi_a)$	-80 ± 50	-0.38 ± 0.03
2	9.56	9.30	$10a_1(\pi_s)$	-30 ± 50	-0.41 ± 0.02
3	11.26	11.36	$3a_2(\pi_{CC})$	0 ± 100	0.05 ± 0.02
4	11.54	11.86	$6b_2(\sigma_{CC})$	-50 ± 100	-0.19 ± 0.02
5	12.18	12.04	$5b_1(\sigma_{CH})$	0 ± 100	-0.13 ± 0.02
6	12.67	12.60	$9a_1(\sigma_{CC})$	-60 ± 100	-0.23 ± 0.05
7	13.05	13.09	$5b_2(\sigma_{CC})$	-50 ± 100	-0.17 ± 0.03
8	13.27	13.23	$8a_1(\sigma_{CH})$	0 ± 100	
9	14.17	13.94	$4b_1(\sigma_{CC})$	-30 ± 50	-0.16 ± 0.03
10	15.74	15.87	$3b_1(\sigma_{CH})$	90 ± 50	-0.06 ± 0.08
11	16.44	16.76	$4b_2(C_{2s})$	0 ± 100	-0.04 ± 0.02
12	17.10	17.34	$7a_1(\sigma_{CH})$	-30 ± 50	-0.03 ± 0.05
13	(18.3)	18.08	$2a_2(C_{2s})$	—	(0.1)

the calculated CEDPICS for ionization from 5e′ and $5a_1'$ MOs extending around the N atoms showed the same negative slope ($m = -0.10$). From the calculated CEDPICS, it is clear that ionization from σ_{CH} orbitals of $1a_1''$ MO ($m = -0.11$) and 3e″ MO ($m = -0.10$), which are out-of-phase between bonded methylene groups, also can be affected by the attractive interaction around N atoms because overlap between 1s orbital of He^* and the corresponding MO vanishes at the nodal plane. On the other hand, ionization from $1a_2'$ MO ($m = 0.06$) and 3e′ MO ($m = 0.12$), which are in-phase between bonded methylene groups, shows the effect of repulsive interaction around the ethylene groups with calculated positive CEDPICS. Since faster He^* atoms can reach the inner reactive region in the case of the head-on collisions against the soft repulsive interaction potential, the ionization cross section shows steeper positive collision energy dependence than that for the collisions against the hard repulsive potential. The positive slope for ionization from $1a_2'$ and 3e′ MOs, therefore, can be ascribed to the soft repulsive potential surface for accessing of a He^* atom to the CH_2–CH_2 region (Fig. 10).

When we focus on the difference of the phase of MOs and slope of CEDPICS for ionization from out-of-phase MO (4e″, $m = 0.09$) and in-phase MO (4e′, $m = -0.03$) between bonded two methylene groups, the larger extension of 4e″ MO around the σ_{CH} bonds than 4e′ MO is more important for the slope of CEDPICS rather than the phase of orbitals around the repulsive ethylene groups. Experimentally, the repulsive interaction around the σ_{CH} bond results in small CEDPICS for band 3 ($m = -0.08 \pm 0.02$), corresponding to ionization from 4e″ MO, which is consistent with the small positive slope of the calculated CEDPICS for ionization from 4e″ MO ($m = 0.09$) when one takes the slope differences between observed and calculated CEDPICS for bands 1, 2, and 4 into consideration.

On the other hand, calculated negative slopes for ionization from the 5e′ MO ($m = -0.10$) and 4e′ MO ($m = -0.03$) are inconsistent with the observed CEDPICS for bands 5,6 ($m = -0.03 \pm 0.05$). In the CERPIES, positive collision energy dependence was observed at ca. 6.8–6.9 eV in the region of bands 5,6. From the estimated values of band 5 (5e′, 6.84 eV) and band 6 (4e′, 6.35 eV), this positive dependence can be ascribed to ionization from the 5e′ MO. Taking the electron density distribution of 5e′ MO into account, this positive collision energy dependence at ca. 6.8–6.9 eV is due to head-on collision with the methylene groups against the repulsive interaction. A softer repulsive interaction potential curve around the methylene groups of DABCO can be expected.

Although the calculated CEDPICS for band 11 shows positive slope ($m = 0.24$) with the repulsive interaction around the σ_{CH} bonds, the observed CEDPICS shows almost no slope ($m \sim 0.0$). A similar difference is obtained for ionization from 4e″ MO for observed ($m = -0.08 \pm 0.02$) and calculated ($m = 0.09$) CEDPICS for band 3. Since the negative CEDPICS can be connected to nitrogen orbitals, the fact that the difference of slope of CEDPICS for band 11 is larger than that

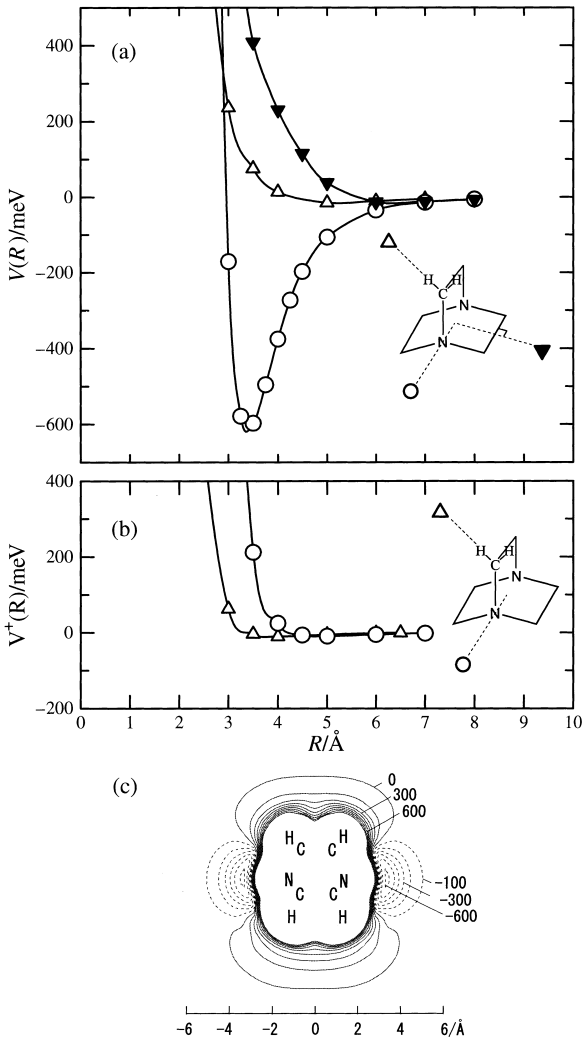

Fig. 10. Interaction potential energy curves for (a) M(DABCO)-Li and (b) the first ionic state of M^+(DABCO)-He: straight access to the center of the molecule along NN axis (○) and around the middle point of CC axis (▼); straight access to the C atom along the CH axis (△). (c) Interaction potential energy contour map for M(DABCO)–Li. Negative energy area is shown by dashed curves and the energy spacing is 100 meV.

for band 4 may be ascribed to some shake-up states having relation to ionization from HOMO or NHOMO, while shake-up states cannot be calculated with the one particle OVGF method.

B. 1,4-Cyclohexadiene. As with the case of DABCO, the energy of antisymmetric MO ($5b_1$, π_a) for two π_{CC} orbitals is more stable than the symmetric MO ($8a_1$, π_s) of 1,4-cyclohexadiene by the through-bond interaction, which was confirmed by the OVGF calculation.[43] As is the case with DABCO, antibonding mixing of σ_{CH} components with the π_s orbital in $8a_1$ MO results in the band intensity for band 1 being smaller than that for band 2 in PIES. For CHD, similar EED values for $8a_1$ orbital (5.81) and $5b_1$ orbital (5.88) were calculated with 6-311++G^{**} basis set in this study as reported with 4-31G basis set.[15] Nodal planes of $8a_1$ orbital can reduce ionization probability from calculated EED values because of no ionization probability at the nodal plane.

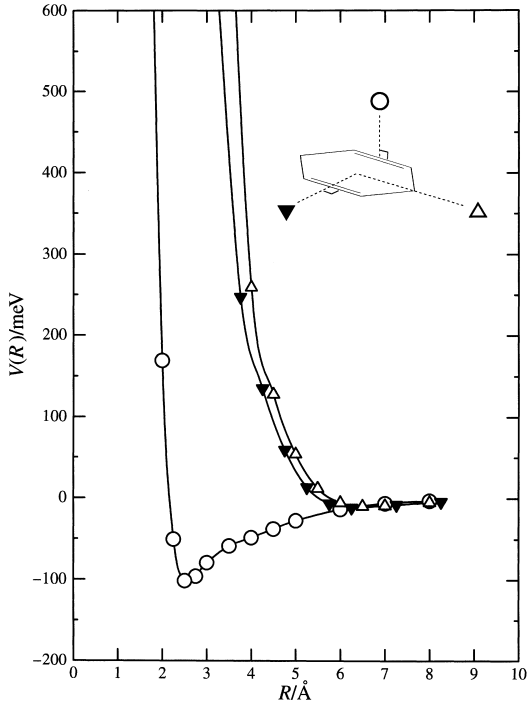

Fig. 11. Interaction potential energy curves for 1,4-cyclohexadiene with Li: in-plane access to the center of the molecule around the CH_2 group (▼) and the middle point of CC axis (△); out-of-plane access to the middle point of C=C (●).

An attractive interaction was calculated for the out-of-plane access to the center of the planar ring (Fig. 11) with a well depth of 100 meV that is smaller than that for 2,5-norbornadiene in the endo region. This attractive interaction can result in the negative slope of the π bands, band 1 (π_s, $m = -0.35 \pm 0.04$) and band 2 (π_a, $m = -0.44 \pm 0.03$). Since the π_s MO has electron density around the σ_{CH} bonds, the smaller slope of CEDPICS for band 1 can be ascribed to the repulsive interaction around the σ_{CH} bonds (Fig. 11), which is the same case as that for DABCO (Section A). In the case of CHD and NBD, trajectory calculations of CEDPICS and comparisons of the results with observed ones are difficult because of the lower symmetry of molecules, although similar trends of CEDPICS can be expected for band 1 and band 2 of the through-bond interaction oriented cases, DABCO and CHD. In addition, it should be noted that the band 1 shows a broader shape than band 2 in PIES.

The CEDPICS of band 3 ($m = -0.06 \pm 0.05$) and band 4 ($m = -0.08 \pm 0.06$) show small negative slopes, reflecting a repulsive interaction around the σ_{CH} bonds for the in-plane direction of the ring and around the methylene groups. Band 5 and band 6 can be ascribed to ionization from the $6b_2$ MO and $5b_2$ MO, respectively. These MOs are in-phase around the σ_{CH} bonds for the half sides of the ring. Very small slope values of CEDPICS for band 5 ($m = -0.01 \pm 0.04$) and band 6 ($m = -0.02 \pm 0.05$) indicate soft repulsive interactions in the interbond region around the molecule for in-plane directions. The soft repulsive interaction for CH_2 region (△) and C=C region (▼) for in-plane direction is shown in Fig. 11. Similar electron

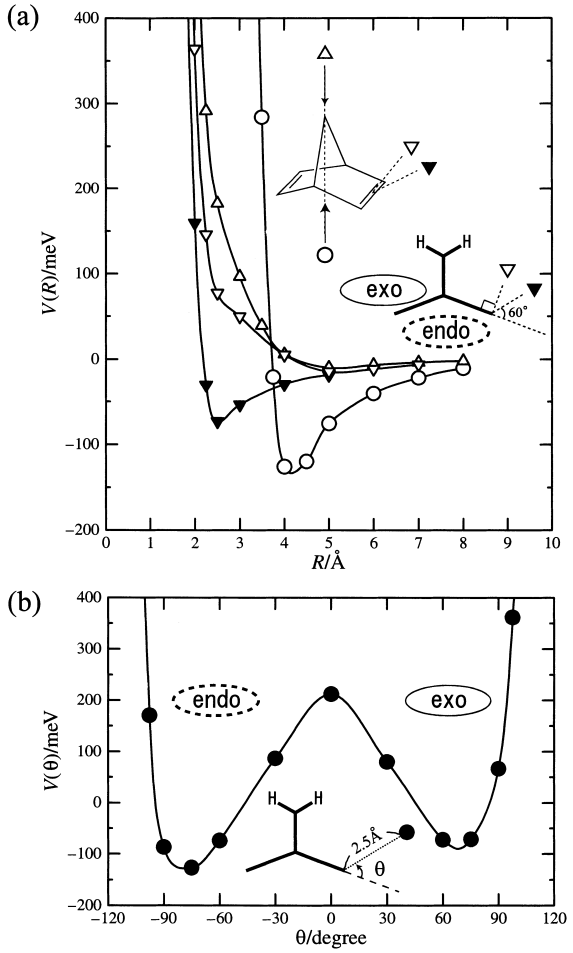

Fig. 12. Interaction potential energy curves for 2,5-norbornadiene with Li: (a) straight access to the CH_2 group in exo region (△) and endo region (○), vertical direction to C=C with the angle of 90 degree (▽) or 60 degree (▼) between Li-X (X is the middle point of C=C bond) and the H–C=C–H plane; (b) as a function of angle between Li–X and the H–C=C–H plane at Li–X distance of 2.5 Å.

density distributions of $7a_1$ (band 4) and of $4b_2$ (band 10) MOs extending outside of the boundary surface of collision result in almost the same slopes of CEDPICS for band 4 ($m = -0.08 \pm 0.06$) and band 10 ($m = -0.07 \pm 0.05$). Band 11 shows small negative collision energy dependence ($m = -0.09 \pm 0.04$), which also can be ascribed to repulsive interaction around the σ_{CH} bonds and attractive interaction at the center of the molecule, because of the in-phase distribution of the $5a_1$ MO around the σ_{CH} bonds and at the center of the molecule, as shown in Fig. 8.

The negative slope of CEDPICS for ionization from the $6a_1$ MO (band 8,9, $m = -0.18 \pm 0.07$) was observed to be somewhat larger than that from the $4b_1$ MO (band 7, $m = -0.09 \pm 0.05$) was observed. It should be noted that ionization probability from the $3b_1$ MO (band 9) is expected to be very small because it has nodal planes and scarcely extends out of the boundary surface of collision. Such difference of the slope of CEDPICS can be caused by the attractive interaction for accessing to the center of the ring where ionization is favorable for the $6a_1$ MO rather than for the $4b_1$ MO that has a nodal plane perpendicular to the molecular plane.

The large intensity of band 12 is not consistent with the small electron density extending of the $2a_2(C_{2s})$ orbital outside the boundary surface of collision, which may be due to the enhancement by intramolecular Auger-like autoionization process.[44] In the case of a previous PIES study for $(CH_3)_4C$ and $(CH_3)_3CCl$, enhanced bands were observed for C_{2s} orbitals; such enhancement was found to be caused by an intermolecular resonant excitation transfer ($He^* + M \rightarrow He + M^*$) involving a C_{2s} hole in the target molecule M followed by an intramolecular Auger-like autoionization process ($M^* \rightarrow M^+ + e^-$).[44] The autoionization process involves an electron transition from an outer occupied C_{2s} MO to the inner C_{2s} hole. For CHD, the OVGF calculation shows that IP values for the C_{2s} orbital can be observed around 24.39 eV ($2b_1$) and 26.46 eV ($3a_1$), which is near the approximate 1s orbital energy (24.59 eV) of $He^*(2^3S)$ obtained from the ionization energy of a He atom. The energy of an unoccupied MO is estimated to be −3.0 eV from the first ionization energy (8.79 eV) and a transition energy (5.80 eV) determined by electron energy loss spectroscopy,[45] this energy value is near to the 2s orbital energy of $He^*(2^3S)$, −4.77 eV (= 19.82 − 24.59). It should be noted, as shown in Fig. 8, that MO coefficients of C_{2s} components are larger for the $2a_2$ MO than for the $4b_2$ MO by 1.7 times in the square of C_{2s} coefficients, which can be the reason of the enhancement of band 12. In addition, for band 12, there may be little possibility of shake-up process from π orbitals because of the different trends of the CEDPICS for π bands ($m = -0.35 \pm 0.04$, -0.44 ± 0.03) and for band 12 ($m \sim 0.0$).

C. 2,5-Norbornadiene. Contrary to the cases in which the through-bond interaction orients (DABCO (Section A) and CHD (Section B)), the energy of the symmetric π_s MO ($6b_1$) for 2,5-norbornadiene (NBD) is more stable than that of the antisymmetric π_a MO ($10a_1$) by the favorable overlapping of two π_{CC} orbitals in the endo region with the through-space intramolecular interaction.

A relatively large negative slope of CEDPICS was observed for ionization from the π_a orbital (band 1, $m = -0.38 \pm 0.03$) and the π_s orbital (band 2, $m = -0.41 \pm 0.02$). As shown in the potential energy calculation (Fig. 12), attractive interactions with a well depth of about 100 meV were calculated for both endo and exo regions. That the intensity of band 2 was larger than that of band 1 was also ascribed to the in-phase MO (π_s) which is related to the through-space interaction in the endo region.[15] That the negative slope of CEDPICS for the π_s orbital (band 2) is larger than that for the π_a orbital (band 1) is also due to the nodal plane of π_a orbital in the endo region where the attractive well depth is larger than that in the exo region. Negative peak shifts of band 1 and band 2 can be ascribed to the attractive interaction around the C=C bonds.

A positive slope value of CEDPICS was observed for band 3 ($m = 0.05 \pm 0.02$). The corresponding $3a_2$ MO scarcely extends outside the boundary surface of collision, which can result in a small intensity in PIES and positive CEDPICS due to the repulsive interaction around the σ_{CH} bonds. In addition, a repulsive interaction was calculated around the methylene group as shown in interaction potential energy curves (Fig. 12(a, b)). The small negative slope values of CEDPICS for

bands 4–9 are caused by corresponding MOs extending into the specific regions of attractive interactions in the end ($6b_2$, $9a_1$, $5b_2$, and $8a_1$ MOs) or exo region ($4b_1$ and $5b_1$ MOs) and repulsive interactions around methylene group ($5b_1$, $8a_1$, and $4b_1$ MOs) or σ_{CH} bonds ($6b_2$, $9a_1$, and $5b_2$ MOs) neighboring the methylene group.

Band 9 ($m = -0.16 \pm 0.03$) and band 10 ($m = -0.06 \pm 0.08$) show different collision energy dependences in spite of the similar type of MOs ($4b_1$ and $3b_1$). Since the $3b_1$ MO has electron density around σ_{CH} bonds, the fact that the negative slope of CEDPICS for band 10 ($3b_1$) is smaller than that for band 9 ($4b_1$) is due to the repulsive interaction around σ_{CH} bonds as shown at 0 degrees in Fig. 12(b).

Band 11 and band 12 show similarly small negative slope values of CEDPICS reflecting the repulsive interaction around the σ_{CH} bonds. The intensity of band 12 is larger than that of band 11 in PIES, which can be interpreted by the in-phase $7a_1$ MO (band 12) outside the boundary surface of collision. On the other hand, the broad band 13 is calculated to be a combination of electron correlation bands ionized from $2a_2$ MO mainly at 17.88 eV and 18.50 eV in IP by two-particle-hole Tamm-Dancoff Green's function approximation (2ph TDA).[46] The large intensity of band 13 in spite of the small electron density extension of $6a_2$ orbital (C_{2s}) outside the boundary surface of collision can be connected with the Auger-like autoionization process discussed in Section B. It should be noted that as shown in Figure 9, coefficients of C_{2s} components are larger for $2a_2$ MO than for $4b_2$ MO by 1.7 times in the square of C_{2s} coefficients, which can be the reason of the enhancement of band 13 as is the case of CHD.

Conclusions

Utilizing the characteristics of collisional ionization, we have investigated anisotropic interactions between $He^*(2^3S)$ and sample molecules (1,4-diazabicyclo[2.2.2]octane (DABCO), 1,4-cyclohexadiene (CHD), and 2,5-norbornadiene (NBD)) by measuring collision energy dependence of partial Penning ionization cross sections (CEDPICS). Due to the differences of electron distributions of HOMO and NHOMO which originate from the through-bond or through-space intramolecular interaction between two functional groups, different trends of CEDPICS were observed for related MOs as follows:

(1) By the through-space interaction, the π_s orbital (NHOMO) of NBD has electron density in the endo region without a nodal plane, which results in the negative slope value of CEDPICS for ionization from NHOMO being larger than that from HOMO. The attractive interaction in the endo region plays an important role.

(2) By the through-bond interaction, symmetric orbitals (n_s or π_s, HOMO) have electron density around the $\sigma_{CC,CH}$ bonds for DABCO and CHD, which results in the negative slope of CEDPICS for ionization from HOMO being lower than that from NHOMO. The repulsive interaction around the $\sigma_{CC,CH}$ orbital region plays an important role.

In the case of DABCO, the theoretically computed CEDPICS based on model potential energy calculations qualitatively agrees with the observed CEDPICS for ionization from HOMO and NHOMO, which indicates that the different trend of CEDPICS is due to the difference in electron distributions of HOMO (n_N with anti-bonding mixing of σ_{CC} component) and NHOMO (n_N with bonding mixing of C_{2s} component). In addition, band 1 in PIES of DABCO shows broad width and different collision energy dependence in the collision-energy-resolved PIES for larger and smaller electron energies, which can be ascribed to ionization from the n_s orbital (HOMO) in both the attractive (nitrogen lone pair orbital) interaction region resulting in smaller electron energy, and the repulsive (σ_{CH} bond) interaction region, resulting in larger electron energy. The synthesized exterior electron density (EED) spectrum of band 1 agrees well with the observed band shape.

This work has been supported by a Grant in Aid for Scientific Research from the Japanese Ministry of Education, Science, Sports and Culture and also partly supported by a Grant in Aid by the CASIO Science Promotion Foundation.

References

1 K. Fukui, "Theory of Orientation and Stereoselection," Springer-Verlag, Berlin (1975).

2 a) R. Hoffmann, A. Imamura, and W. J. Hehre, *J. Am. Chem. Soc.*, **90**, 1499 (1968). b) R. Hoffmann, *Acc. Chem. Res.*, **4**, 1 (1971).

3 a) P. Bishof, J. A. Hashmall, E. Heilbronner, and V. Hornung, *Helv. Chim. Acta*, **52**, 1745 (1969). b) E. Heilbronner and K. A. Muskat, *J. Am. Chem. Soc.*, **92**, 3818 (1970). c) E. Heilbronner and H. D. Martin, *Helv. Chim. Acta*, **55**, 1490 (1970). d) E. Heilbronner, *Helv. Chim. Acta*, **60**, 2248 (1977).

4 a) R. Gleiter, *Angew. Chem.*, **86**, 770 (1974). b) P. Bischof, R. Gleiter, and R. Haider, *J. Am. Chem. Soc.*, **100**, 1036 (1978).

5 a) E. Lindholm, C. Fridh and L. Åsbrink, *Faraday Disc. Chem. Soc.*, **54**, 127 (1972). b) W. von Niessen and G. H. F. Diercksen, *J. Electron Spec. Relat. Phenom.*, **16**, 351 (1979). c) A. Imamura, M. Ohsaku, and K. Akagi, *Tetrahedron*, **39**, 1291 (1983). d) V. Galasso, *Chem. Phys.*, **138**, 231 (1989).

6 H. Hotop and A. Niehaus, *Z. Phys.*, **228**, 68 (1969).

7 V. Čermák, *J. Chem. Phys.*, **44**, 3781 (1966).

8 A. Niehaus, *Adv. Chem. Phys.*, **45**, 399 (1981).

9 A. J. Yencha, "Electron Spectroscopy: Theory, Technique, and Applications," ed by C. R. Brundle and A. D. Baker, Academic, New York (1984), Vol. 5.

10 K. Ohno, H. Mutoh, and Y. Harada, *J. Am. Chem. Soc.*, **105**, 4555 (1983).

11 K. Ohno and Y. Harada, "Theoretical Models of Chemical Bonding, Part 3" ed by Z. B. Maksič, Springer, Berlin (1991).

12 K. Ohno, S. Matsumoto, and Y. Harada, *J. Chem. Phys.*, **81**, 4447(1984).

13 T. Kajiwara, S. Masuda, K. Ohno, and Y. Harada, *J. Chem. Soc. Perkin trans. 2*, **1988**, 507.

14 M. Aoyama, S. Masuda, K. Ohno, Y. Harada, M. C. Yew, H. H. Hua, and L.S. Yong, *J. Phys. Chem.*, **93**, 1800 (1989).

15 K. Ohno, T. Ishida, Y. Naitoh, and Y. Izumi, *J. Am. Chem. Soc.*, **107**, 8082 (1985).

16 K. Ohno, H. Yamakado, T. Ogawa, and T. Yamata, *J. Chem. Phys.*, **105**, 7536 (1996).

17 a) K. Imura, N. Kishimoto, and K. Ohno, *J. Phys. Chem. A*, **105**, 4189 (2001). b) K. Imura, N. Kishimoto, and K. Ohno, *J. Phys. Chem. A*, **105**, 6073 (2001). c) K. Imura, N. Kishimoto, and

K. Ohno, *J. Phys. Chem. A*, **105**, 6378 (2001). d) K. Imura, N. Kishimoto, and K. Ohno, *J. Phys. Chem. A*, **105**, 9111 (2001).

18 K. Ohno, T. Takami, K. Mitsuke, and T. Ishida, *J. Chem. Phys.*, **94**, 2675 (1991).

19 T. Takami, K. Mitsuke, and K. Ohno, *J. Chem. Phys.*, **95**, 918(1991).

20 T. Takami and K. Ohno, *J. Chem. Phys.*, **96**, 6523 (1992).

21 J. L. Gardner and J. A. R. Samson, *J. Electron Spectrosc. Relat. Phenom.*, **8**, 469 (1976).

22 K. Kimura, S. Katsumata, Y. Achiba, T. Yamazaki, and S. Iwata, "Handbook of He I Photoelectron Spectra of Fundamental Organic Molecules," Japan Scientific Press, Tokyo (1981).

23 D. W. Turner, C. Baker, A. D. Baker, and C. R. Brundle, "Molecular Photoelectron Spectroscopy," Wiley, London (1970).

24 D. S. C. Yee, W. B. Stewart, C. A. Mcdowell, and C. E. Brion, *J. Electron Spectrosc. Relat. Phenom.*, **7**, 93 (1975).

25 H. Hotop and G. Hübler, *J. Electron Spectrosc. Relat. Phenom.*, **11**, 101 (1977).

26 a) D. J. Auerbach, "Atomic and Molecular Beam Methods," ed by G. Scoles, Oxford University, New York (1988), p. 369. b) N. Kishimoto, J. Aizawa, H. Yamakado, and K. Ohno, *J. Phys. Chem. A*, **101**, 5038 (1997).

27 A. Yokozeki and K. Kuchitsu, *Bull. Chem. Soc. Jpn.*, **44**, 72 (1971).

28 G. Dallinga and L. H. Toneman, *J. Mol. Struct.*, **1**, 117 (1967).

29 W. von Niessen and G. H. F. Diercksen, *J. Electron Spectrosc. Relat. Phenom.*, **16**, 351 (1979).

30 L. Pauling, "The Nature of the Chemical Bond," Cornell University, Ithaca, New York (1960).

31 V. G. Zakrzewski and J. V. Ortiz, *Int. J. Quantum Chem.*, **53**, 583 (1995).

32 M. J. Frisch, G. W. Trucks, H. B. Schlegel, P. M. W. Gill, B. G. Johnson, M. A. Robb, J. R. Cheeseman, T. Keith, G. A. Petersson, J. A. Montgomery, K. Raghavachari, M. A. Al-Laham, V. G. Zakrzewski, J. V. Ortiz, J. B. Foresman, J. Cioslowski, B. B. Stefanov, A. Nanayakkara, M. Challacombe, C. Y. Peng, P. Y. Ayala, W. Chen, M. W. Wong, J. L. Andres, E. S. Replogle, R. Gomperts, R. L. Martin, D. J. Fox, J. S. Binkley, D. J. Defrees, J. Baker, J. P. Stewart, M. Head-Gordon, C. Gonzalez, and J. A. Pople, "Gaussian 94 (Revision C. 3)," Gaussian, Inc., Pittsburgh PA (1995).

33 E. W. Rothe, R. H. Neynaber, and S. M. Trujillo, *J. Chem. Phys.*, **42**, 3310 (1965).

34 H. Hotop, *Radiat. Res.*, **59**, 379 (1974).

35 H. Haberland, Y. T. Lee, and P. E. Siska, *Adv. Chem. Phys.*, **45**, 487 (1981).

36 E. Illenberger and A. Niehaus, *Z. Phys. B*, **20**, 33 (1975).

37 T. Parr, and D. M. Parr, *J. Chem. Phys.*, **76**, 316 (1982).

38 H. Hotop, T. E. Roth, M.-W. Ruf, and A. J. Yencha, *Theor. Chem. Acc.*, **100**, 36 (1998).

39 a) T. Ogawa and K. Ohno, *J. Chem. Phys.*, **110**, 3773 (1999). b) T. Ogawa and K. Ohno, *J. Phys. Chem. A*, **103**, 9925 (1999).

40 T. Ishida and K. Ohno, *Int. J. Quant. Chem.*, **32**, 257 (1989).

41 a) M. Takahashi, R. Ogino, and Y. Udagawa, *Chem. Phys. Lett.*, **288**, 714 (1998). b) M. Takahashi, M. Matsuo, and Y. Udagawa, *Chem. Phys. Lett.*, **308**, 195 (1999).

42 E. Weigold and I. E. McCarthy, "Electron Momentum Spectroscopy," Kluwer Academic/Plenum Publishers, New York (1999).

43 M. H. Palmer, *J. Mol. Struct.*, **161**, 333 (1987).

44 T. Takami, K. Mitsuke, and K. Ohno, *J. Chem. Phys.*, **95**, 918 (1991).

45 R. McDiarmid and J. P. Doering, *J. Chem. Phys.*, **75**, 2687 (1981).

46 G. Bieri, L. Åsbrink, and W. von Niessen, *J. Electron Spectrosc. Relat. Phenom.*, **27**, 129 (1982).